

Structures and stability of calcium and magnesium carbonates at mantle pressures

Chris J. Pickard*

*Department of Physics & Astronomy, University College London, Gower Street, London WC1E 6BT, UK
London Institute for Mathematical Sciences, 35a South Street, Mayfair, London, W1K 2XF, UK*

Richard J. Needs

*Theory of Condensed Matter Group, Cavendish Laboratory,
J J Thomson Avenue, Cambridge CB3 0HE, UK*

(Dated: March 2, 2022)

Ab initio random structure searching (AIRSS) and density functional theory methods are used to predict structures of calcium and magnesium carbonate (CaCO_3 and MgCO_3) at high pressures. We find a previously unknown CaCO_3 structure which is more stable than the aragonite and “post aragonite” phases in the range 32–48 GPa. At pressures from 67 GPa to well over 100 GPa the most stable phase is a previously unknown CaCO_3 structure of the pyroxene type with fourfold coordinated carbon atoms. We also predict a stable structure of MgCO_3 in the range 85–101 GPa. Our results lead to a revision of the phase diagram of CaCO_3 over more than half the pressure range encountered within the Earth’s mantle, and smaller changes to the phase diagram of MgCO_3 . We predict CaCO_3 to be more stable than MgCO_3 in the Earth’s mantle above 100 GPa, and that CO_2 is not a thermodynamically stable compound under deep mantle conditions. Our results have significant implications for understanding the Earth’s deep carbon cycle.

PACS numbers: 64.70.K-, 71.15.Mb, 61.50.Ks, 62.50.-p

I. INTRODUCTION

The occurrence of CO_2 within magmas and volcanic gases indicates a significant carbon presence within the Earth’s lower mantle^{1,2}. Carbon has a low solubility in mantle silicates and the majority of the oxidized carbon in the Earth’s mantle is believed to exist in the form of carbonates. Calcium and magnesium carbonate (CaCO_3 and MgCO_3) are the main sources and sinks of atmospheric CO_2 within the Earth’s mantle. Carbonates are conveyed into the deep Earth by subduction, and carbon is recycled to the surface via volcanic processes in the form of CO_2 -containing fluids and solids, and diamonds^{3,4}. However, the details of carbon storage within the Earth’s interior are unclear. The Deep Carbon Observatory⁵ has been set up to investigate carbon within the Earth’s deep interior. CaCO_3 and MgCO_3 play fundamental roles in the global carbon cycle and influence the climate of our planet^{6,7}. Knowledge of the structures, energetics and other properties of CaCO_3 and MgCO_3 at high pressures is therefore important in understanding the Earth’s mantle, and especially the carbon cycle.

The low-pressure calcite form⁸ of CaCO_3 is one of the most abundant minerals on the Earth’s surface and is the main constituent of metamorphic marbles. Several metastable calcite-like phases have been observed^{9–11}, and a calcite-related phase has been reported at around 25 GPa^{11,12}. At pressures of about 2 GPa calcite transforms to the aragonite structure¹³ of $Pnma$ symmetry. At about 40 GPa aragonite transforms into the “post aragonite” ($Pmmn$) structure of CaCO_3 , which is stable up to at least 86 GPa^{14,15}. The low pressure magnesite phase of MgCO_3 has the same structure as calcite.

Experiments indicate that magnesite is stable up to 80 GPa¹⁶, and a phase transition occurs above 100 GPa to an unknown magnesite II structure^{17,18}.

II. STRUCTURE SEARCHES

Density functional theory (DFT) calculations for high pressure phases of CaCO_3 and MgCO_3 were performed by Oganov *et al.* using an evolutionary structure searching algorithm^{15,19}. These calculations predicted a transition from the calcite to aragonite to “post aragonite” structures of CaCO_3 , followed by a transition to a structure of $C222_1$ symmetry at pressures over 100 GPa. Similar calculations for MgCO_3 predicted transitions from magnesite to a structure of $C2/m$ symmetry at 82 GPa, followed by a transition to a structure of $P2_1$ symmetry at 138 GPa, and a phase of $Pna2_1$ symmetry at 160 GPa¹⁹.

Calculations using the *ab initio* random structure searching (AIRSS) technique²⁰ have led to the discovery of structures that have subsequently been verified by experiment, for example, in silane²¹, aluminium hydride²², ammonia monohydrate²³ and ammonia dihydrate²⁴. In the basic AIRSS approach a cell volume and shape is selected at random from within reasonable ranges, the atoms are added at random positions, and the system is relaxed until the forces on the atoms are negligible and the pressure takes the required value. This procedure is repeated many times, leading to a reasonably unbiased scheme which allows a significant portion of the “structure space” to be investigated, although the sampling may be rather sparse. This approach is often successful for small systems, but it involves sampling a large portion

of the high-energy structure space which is not normally of interest. We therefore reduce the size of the structure space investigated by constraining the searches.

We first perform searches in small cells, constraining the initial structures so that all of the atoms are at least 1 Å apart. The low-enthalpy structures obtained from these calculations give us information about the favorable bonding configurations and likely nearest neighbor distances between the different atomic types. At low pressures we find that the low-enthalpy structures contain well-defined triangular CO_3 or ring C_3O_9 units, and therefore we place these units and Ca or Mg atoms randomly within the cells of random shapes. We ensure that the atoms are not too close together by constraining the initial values of the minimum distances between atoms for each of the six possible pairs of atomic species. The six minimum distances are obtained from low-enthalpy structures found in the small-cell searches. To construct the initial structures at higher pressures we use minimum distances from low-enthalpy small-cell structures to prepare new larger structures that approximately satisfy the minimum distance constraints. This approach helps to space out the different species appropriately, while retaining a high degree of randomness. We perform searches at both low and high pressures, using structures which are constrained to have a certain symmetry which is enforced during the relaxation, but are otherwise random²⁰. This approach is useful because low energy structures often possess symmetry^{25,26}, although symmetry constraints break up the allowed structure space into disconnected regions and can prevent some structures from relaxing to lower energy ones²⁰. We consider structures containing up to eight formula units (f.u.) for CaCO_3 and twelve f.u. for MgCO_3 .

Our first-principles DFT calculations are performed using the CASTEP plane-wave basis set pseudopotential code²⁷. We use the Perdew-Burke-Ernzerhof (PBE) generalized gradient approximation (GGA) density functional²⁸, default CASTEP ultrasoft pseudopotentials²⁹, and a plane-wave basis set energy cutoff of 440 eV. We use a Brillouin zone sampling grid of spacing $2\pi \times 0.1 \text{ \AA}^{-1}$ for the searches, and a finer spacing of $2\pi \times 0.05 \text{ \AA}^{-1}$ for the final results reported in this paper.

III. CaCO_3 , PRESSURE ≤ 50 GPa

Calculated enthalpy-pressure curves for CaCO_3 phases are shown in Fig. 1, relative to the enthalpy of the “post aragonite” phase. The transition from aragonite to “post aragonite” becomes energetically favorable at about 42 GPa, in agreement with previous DFT results^{15,19,30,31} and experiment¹⁴. We performed calculations for the CaCO_3 -VI structure reported in Ref. 11, which was suggested as a possible high pressure phase of CaCO_3 . However, we found it to be very high in enthalpy, with a strongly anisotropic stress and large forces on the atoms.

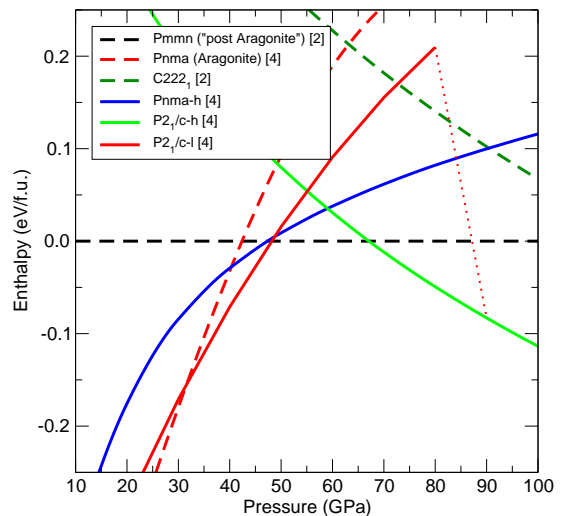


FIG. 1. (Color online) Enthalpies per f.u. of CaCO_3 phases relative to “post aragonite”, with the number of f.u. per primitive unit cell given within square brackets. The enthalpies of phases known prior to the current study are shown as dashed lines, while those found in the current study are shown as solid lines. The dotted red line shows the collapse of the CaCO_3 - $P2_1/c-l$ structure into the more stable CaCO_3 - $P2_1/c-h$ structure at 80–90 GPa.

Relaxation of the CaCO_3 -VI structure at 40 GPa led to a reasonably stable structure with an enthalpy close to that of aragonite, but the relaxed structure does not have a region of stability on our phase diagram (Fig. 1). We also found a structure of $Pnma$ symmetry (“ CaCO_3 - $Pnma-h$ ”, where h denotes “high pressure”) that is predicted to be more stable than aragonite above 40 GPa, and more stable than “post aragonite” below 47 GPa. However, CaCO_3 - $Pnma-h$ does not have a region of thermodynamic stability on our phase diagram because we find a previously unknown structure of $P2_1/c$ symmetry (“ CaCO_3 - $P2_1/c-l$ ”, where l denotes “low pressure”) which is calculated to be the most stable phase in the pressure range 32–48 GPa, see Fig. 1.

At 42 GPa CaCO_3 - $P2_1/c-l$ is calculated to be about 0.05 eV per f.u. more stable than aragonite and “post aragonite” and, because these sp^2 bonded structures are similar, we expect that DFT calculations should give rather accurate enthalpy differences between them. However, our CaCO_3 - $P2_1/c-l$ and CaCO_3 - $Pnma-h$ structures do not provide as good a fit to the experimental X-ray diffraction data as the “post aragonite” phase¹⁵. It is possible that large energy barriers hinder formation of the CaCO_3 - $P2_1/c-l$ structure. Another possibility is that the laser-heated sample melts and the least stable polymorph crystallizes from the melt first, in analogy to “Ostwald’s rule”³². In any case, the conditions within the Earth’s mantle are not the same as in diamond anvil cell experiments, and the timescales associated with geological processes are enormously longer than those for laboratory experiments.

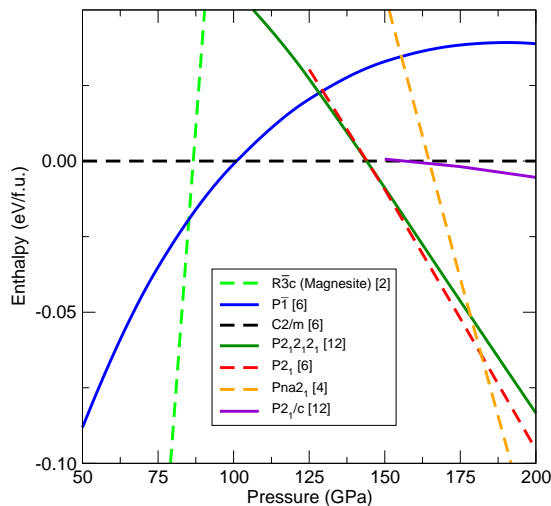


FIG. 2. (Color online) Enthalpies per f.u. of MgCO_3 phases relative to the $C2/m$ phase, with the number of f.u. per primitive unit cell given within square brackets. Previously known phases are shown as dashed lines, and those found in the current study are shown as solid lines.

IV. CaCO_3 , PRESSURE > 50 GPa

At higher pressures we find another CaCO_3 structure of $P2_1/c$ symmetry (“ $\text{CaCO}_3\text{-}P2_1/c\text{-}h$ ”) to be stable from 67 GPa to well above 100 GPa. Our $\text{CaCO}_3\text{-}P2_1/c\text{-}h$ structure is about 0.18 eV per f.u. more stable than the $C222_1$ structure found by Oganov *et al.*¹⁵, see Fig. 1, and $C222_1$ does not have a region of thermodynamic stability. We also find that at about 80–90 GPa $\text{CaCO}_3\text{-}P2_1/c\text{-}l$ transforms into the more stable $\text{CaCO}_3\text{-}P2_1/c\text{-}h$ structure without any apparent energy barrier (dotted red line in Fig. 1). Our calculations lead to the prediction of a new and more stable polymorph of CaCO_3 at pressures > 67 GPa.

V. MgCO_3

Calculated enthalpy-pressure curves for MgCO_3 phases in the pressure range 50–200 GPa are shown in Fig. 2, relative to the $C2/m$ phase. We find a previously unreported structure of $P1$ symmetry to be the most stable in the range 85–101 GPa. We also find a phase of $P2_12_12_1$ symmetry that is marginally the most stable at pressures around 144 GPa, see Fig. 2.

VI. STRUCTURES AND BONDING

The carbon atoms in the calcite, aragonite, “post aragonite”, and our $\text{CaCO}_3\text{-}P2_1/c\text{-}l$ and $\text{CaCO}_3\text{-}Pnma\text{-}h$ structures contain threefold coordinated carbon atoms, as does the magnesite phase of MgCO_3 . These structures

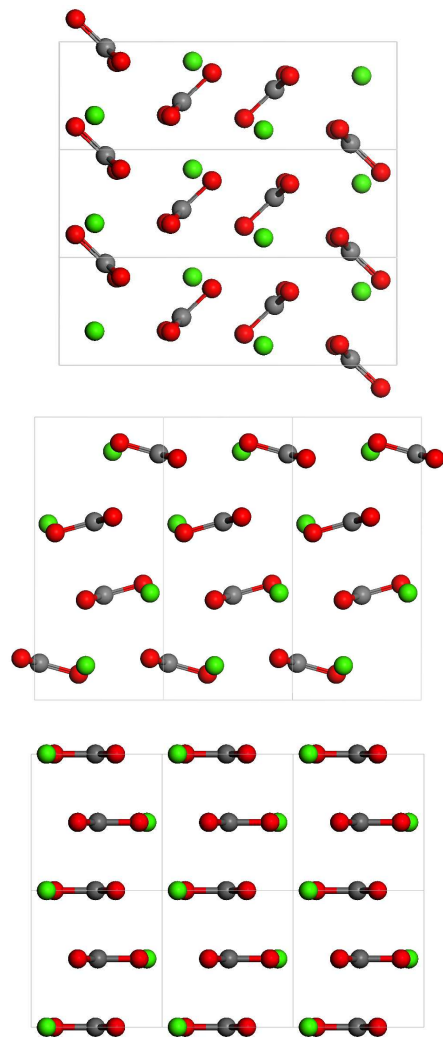


FIG. 3. (Color online) The $\text{CaCO}_3\text{-}P2_1/c\text{-}l$ (top), $\text{CaCO}_3\text{-}Pnma\text{-}h$ (middle), and “post aragonite” (bottom) structures of CaCO_3 at 40 GPa. The Ca atoms are in green, the carbon in grey, and the oxygen in red.

contain triangular CO_3^{2-} ions with sp^2 bonding. In aragonite and “post aragonite” the CO_3^{2-} ions are coplanar, but in our $\text{CaCO}_3\text{-}Pnma\text{-}h$ structure they are somewhat tilted, while in $\text{CaCO}_3\text{-}P2_1/c\text{-}l$ they are tilted at approximately 90° to one another, see Fig. 3. More details of the structures are given in the Supplemental Material³³.

The high-pressure $\text{CaCO}_3\text{-}P2_1/c\text{-}h$ and $C222_1$ structures contain fourfold coordinated carbon atoms and are of the pyroxene type. $\text{CaCO}_3\text{-}P2_1/c\text{-}h$ and $C222_1$ possess very similar calcium lattices but the packing of the pyroxene chains is different, as can be seen in Fig. 4. In $C222_1$ each of the chains is orientated in the same manner, but $\text{CaCO}_3\text{-}P2_1/c\text{-}h$ alternate chains run in the reverse direction, see Fig. 4, and consequently the unit cell of $\text{CaCO}_3\text{-}P2_1/c\text{-}h$ contains four f.u., whereas $C222_1$ contains two. When viewed along the axis of the chains, the $\text{CaCO}_3\text{-}P2_1/c\text{-}h$ and $C222_1$ structures appear almost identical. $\text{CaCO}_3\text{-}P2_1/c\text{-}h$ and $C222_1$ have very simi-

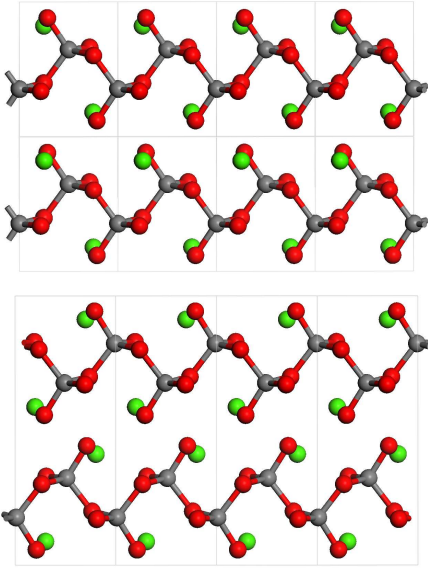


FIG. 4. (Color online) The $C222_1$ (top) and $\text{CaCO}_3\text{-}P2_1/c\text{-}h$ pyroxene-type (bottom) structures of CaCO_3 at 60 GPa. The Ca atoms are in green, carbon in grey, and oxygen in red.

lar volumes at high pressures, with $C222_1$ being slightly denser, which leads to almost parallel enthalpy-pressure relations, see Fig. 1. The lower enthalpy of $\text{CaCO}_3\text{-}P2_1/c\text{-}h$ must therefore arise from more favorable electrostatic interactions between the pyroxene chains.

A. High-pressure X-ray data for CaCO_3

Ono *et al.*³⁴ performed laser-heated diamond anvil cell experiments on CaCO_3 at 182 GPa. X-ray diffraction data for the $C222_1$ ¹⁵ and $\text{CaCO}_3\text{-}P2_1/c\text{-}h$ structures are compared in Fig. 5 with the experimental data from Fig. 1 of Ref. 34. Note the appearance of three peaks marked with stars in the experimental data that arise from the platinum used to enhance heat absorption during the laser heating and as a pressure calibrant. The experimental data is not of very high resolution. The diffraction patterns of the theoretical $C222_1$ and $\text{CaCO}_3\text{-}P2_1/c\text{-}h$ structures share many common features. There are also clear similarities between the theoretical and experimental X-ray data, but the experimental data is of insufficient resolution to allow the structure to be determined unambiguously. We suggest that our $\text{CaCO}_3\text{-}P2_1/c\text{-}h$ structure is the best available candidate for the observed high pressure phase because it has a much lower enthalpy than $C222_1$.

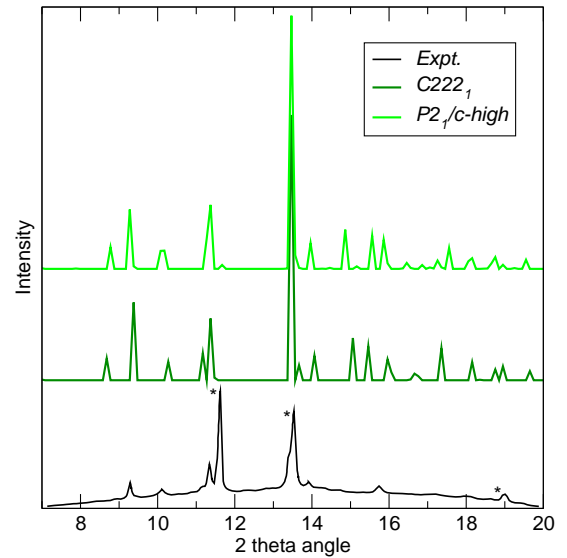


FIG. 5. (Color online) X-ray diffraction patterns of the $C222_1$ ¹⁵ and $\text{CaCO}_3\text{-}P2_1/c\text{-}h$ phases of CaCO_3 , compared with experimental data from Fig. 1(b) of Ref. 34. Data at 182 GPa are reported, with an incident wavelength of 0.415 Å. The stars indicate that the peak immediately to the right arises from platinum.

VII. CHEMICAL REACTIONS IN EARTH'S MANTLE

We have investigated possible chemical reactions involving the mantle materials CaCO_3 , MgCO_3 , CO_2 , MgSiO_3 , CaSiO_3 , SiO_2 , CaO and MgO , following the approach of Oganov *et al.*¹⁹. The most stable structures of each compound at the relevant pressures are used, as provided by DFT studies. We use the $Pa\bar{3}$, $P4_2/mnm$, and $I\bar{4}2d$ structures of CO_2 ³⁵, the stishovite, CaCl_2 and pyrite structures of SiO_2 ³⁶, the rocksalt structure of MgO , the orthorhombic structure of perovskite CaSiO_3 and the perovskite and post-perovskite structures of MgSiO_3 ^{37–39}.

Decomposition of CaCO_3 and MgCO_3 into the alkaline earth oxides plus CO_2 is found to be unfavorable. Under conditions of excess SiO_2 , the reaction



is found to be energetically unfavorable up to 138 GPa, which is just above the pressure at the mantle-core boundary, see Fig. 6. We find that the reaction



does not occur below 200 GPa, see Fig. 7, which is much higher than the value of 135 GPa reported in Ref. 19. We conclude that both MgCO_3 and CaCO_3 are stable within the Earth's mantle under conditions of excess SiO_2 . These results suggest that free CO_2 does not occur as an equilibrium phase within the Earth's mantle.

MgCO_3 has generally been believed to be the dominant carbonate throughout the Earth's mantle. This

assumption can be tested when excess MgO is present by determining the relative stability of $\text{CaCO}_3 + \text{MgO}$ and $\text{MgCO}_3 + \text{CaO}$. We find that $\text{CaCO}_3 + \text{MgO}$ is the more stable up to pressures of about 200 GPa, so that CaCO_3 is the stable carbonate under these conditions. In the case of excess MgSiO_3 we consider the reaction



finding that CaCO_3 is more stable than MgCO_3 from 100 GPa up to pressures well above those of 136 GPa found at the mantle-core boundary, see Fig. 8.

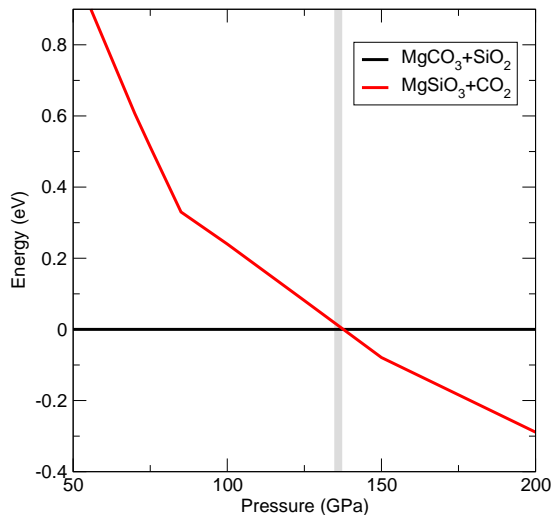


FIG. 6. (Color online). The relative stabilities per f.u. as a function of pressure of $\text{MgCO}_3 + \text{SiO}_2$ and $\text{MgSiO}_3 + \text{CO}_2$. The vertical gray line indicates the pressure at the base of the mantle (136 GPa). In this and the following figures, the kinks arise from phase transitions.

VIII. CONCLUSIONS

In conclusion, we have searched for structures of CaCO_3 and MgCO_3 at mantle pressures using AIRSS^{20,21}. We have found a CaCO_3 - $P2_1/c-l$ structure with sp^2 bonded carbon atoms that is predicted to be stable within the range 32–48 GPa. We have also found a high pressure CaCO_3 - $P2_1/c-h$ structure with sp^3 bonded carbon atoms that is about 0.18 eV per f.u. more stable than the $C222_1$ phase proposed by Oganov *et al.*¹⁵. Both the CaCO_3 - $P2_1/c-h$ and $C222_1$ structures are compatible with the available X-ray diffraction data³⁴. However, CaCO_3 - $P2_1/c-h$ is the most stable structure from 67 GPa to pressures well above those encountered within the Earth's lower mantle (≤ 136 GPa). Our AIRSS calculations suggest a previously unknown phase of MgCO_3 of $P\bar{1}$ symmetry that is predicted to be thermodynamically stable in the pressure range 85–101 GPa. Our results suggest that CO_2 is not a thermodynamically stable compound under deep mantle conditions. Under conditions of excess MgSiO_3 we find that CaCO_3 is more stable

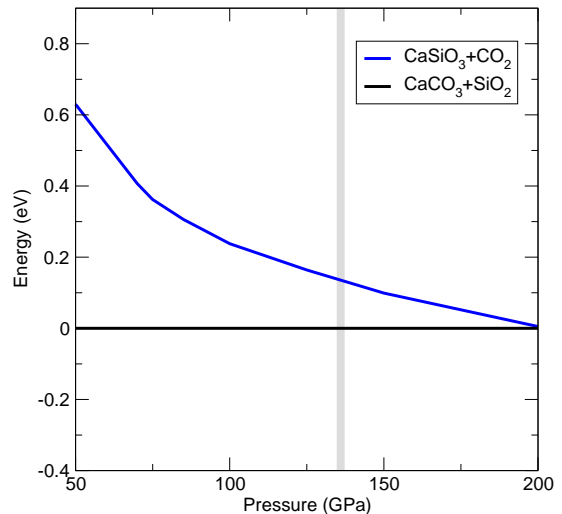


FIG. 7. (Color online). The relative stabilities per f.u. as a function of pressure of $\text{CaSiO}_3 + \text{CO}_2$ and $\text{CaCO}_3 + \text{SiO}_2$. The vertical gray line indicates the pressure at the base of the mantle (136 GPa).

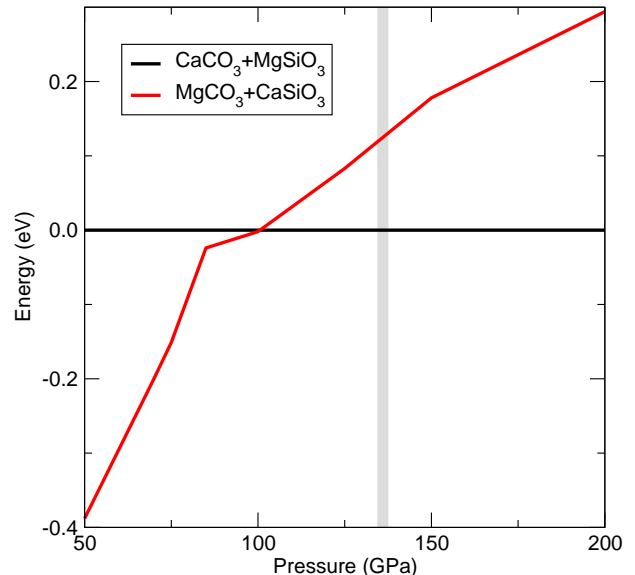


FIG. 8. (Color online) Enthalpy per f.u. of $\text{CaCO}_3 + \text{MgSiO}_3$ compared with that of $\text{CaSiO}_3 + \text{MgCO}_3$. Below 100 GPa we find that $\text{CaSiO}_3 + \text{MgCO}_3$ is the most stable, while above 100 GPa $\text{CaCO}_3 + \text{MgSiO}_3$ is the most stable.

than MgCO_3 above 100 GPa. This result arises directly from our discovery of the highly stable CaCO_3 - $P2_1/c-h$ phase. The results of our study change our understanding of the carbon cycle in the lower part of the mantle and may have important consequences for geodynamics^{40–42} and geochemistry^{43,44}.

ACKNOWLEDGMENTS

We acknowledge financial support from the Engineering and Physical Sciences Research Council (EPSRC) of the United Kingdom.

-
- * c.pickard@ucl.ac.uk
- ¹ B. Marty and A. Jambon, *Earth Planet. Sci. Lett.* **83**, 16 (1987).
 - ² A. N. Halliday, *Geochimica et Cosmochimica Acta* **105**, 146 (2013).
 - ³ S. Ghosh, E. Ohtani, K. D. Litasov, and H. Terasaki, *Chemical Geology* **262**, 17 (2009).
 - ⁴ M. L. Frezzotti, J. Selverstone, Z. D. Sharp, and R. Compagnoni, *Nature Geoscience* **4**, 703 (2011).
 - ⁵ <http://deepcarbon.net/>.
 - ⁶ R. Dasgupta and M. M. Hirschmann, *Earth Planet. Sci. Lett.* **298**, 1 (2010).
 - ⁷ Robert M. Hazen and Craig M. Schiffrin, *Reviews in Mineralogy and Geochemistry* **75**, 1-6 (2013).
 - ⁸ W. L. Bragg, *Proc. R. Soc. Lond. A* **89**, 468 (1914).
 - ⁹ P. W. Bridgman, *American Journal of Science* **237**, 7 (1939).
 - ¹⁰ K. Suito, J. Namba, T. Horikawa, Y. Taniguchi, N. Daku-raos, M. Kobayashi, A. Onodera, O. Shimomura, and T. Kikegawa, *Am. Mineral.* **86**, 997 (2001).
 - ¹¹ M. Merlini, M. Hanfland, and W. A. Crichton, *Earth Planet. Sci. Lett.* **333**, 265 (2012).
 - ¹² K. Catalli and Q. Williams, *Am. Mineral.* **90**, 1679 (2005).
 - ¹³ W. L. Bragg, *Proc. R. Soc. Lond. A* **105**, 16 (1924).
 - ¹⁴ S. Ono, T. Kikegawa, Y. Ohishi, and J. Tsuchiya, *Am. Mineral.* **90**, 667 (2005).
 - ¹⁵ A. R. Oganov, C. W. Glass, and S. Ono, *Earth Planet. Sci. Lett.* **241**, 95 (2006).
 - ¹⁶ Guillaume Fiquet, Francois Guyot, Martin Kunz, Jan Matas, Denis Andrault, and Michael Hanfland, *Am. Mineral.* **87**, 1261-1265 (2002).
 - ¹⁷ Maiko Isshiki, Tetsuo Irifune, Kei Hirose, Shigeaki Ono, Yasuo Ohishi, Tetsu Watanuki, Eiji Nishibori, Masaki Takata, and Makoto Sakata, *Nature* **427**, 60-63 (2004).
 - ¹⁸ Eglantine Boulard, Alexandre Gloter, Alexandre Corgne, Daniele Antonangeli, Anne-Line Auzende, Jean-Philippe Perrillat, Francois Guyot, and Guillaume Fiquet, *Proc. Natl. Acad. Sci. USA* **108**, 5184 (2011).
 - ¹⁹ A. R. Oganov, S. Ono, Y. Ma, C. W. Glass, and A. Garcia, *Earth Planet. Sci. Lett.* **273**, 38 (2008).
 - ²⁰ C. J. Pickard and R. J. Needs, *J. Phys.: Condens. Matter* **23**, 053201 (2011).
 - ²¹ C. J. Pickard and R. J. Needs, *Phys. Rev. Lett.* **97**, 045504 (2006).
 - ²² C. J. Pickard and R. J. Needs, *Phys. Rev. B* **76**, 144114 (2007).
 - ²³ A. D. Fortes, E. Suard, M.-H. Lemee-Cailleau, C. J. Pickard, and R. J. Needs, *J. Am. Chem. Soc.* **131**, 13508 (2009).
 - ²⁴ G. I. G. Griffiths, A. D. Fortes, C. J. Pickard, and R. J. Needs, *J. Chem. Phys.* **136**, 174512 (2012).
 - ²⁵ L. Pauling, *J. Am. Chem. Soc.* **51**, 1010 (1929).
 - ²⁶ D. J. Wales, *Chem. Phys. Lett.* **285**, 330 (1998).
 - ²⁷ S. J. Clark, M. D. Segall, C. J. Pickard, P. J. Hasnip, M. I. J. Probert, K. Refson, and M. C. Payne, *Z. Kristallogr.* **220**, 567 (2005).
 - ²⁸ J. P. Perdew, K. Burke, and M. Ernzerhof, *Phys. Rev. Lett.* **77**, 3865 (1996).
 - ²⁹ D. Vanderbilt, *Phys. Rev. B* **41**, 7892 (1990).
 - ³⁰ S. Arapan, J. S. de Almeida, and R. Ahuja, *Phys. Rev. Lett.* **98**, 268501 (2007).
 - ³¹ S. Arapan and R. Ahuja, *Phys. Rev. B* **82**, 184115 (2010).
 - ³² W. Ostwald, *Zeitschrift für Physikalische Chemie* **22**, 289 (1897).
 - ³³ See Supplemental Material at <http://link.aps.org/supplemental/.....> for details of the structures.
 - ³⁴ S. Ono, T. Kikegawa, and Y. Ohishi, *Am. Mineral.* **92**, 1246 (2007).
 - ³⁵ Cheng Lu, Maosheng Miao, and Yanming Ma, *J. Am. Chem. Soc.* **135**, 14167-14171 (2013).
 - ³⁶ B. B. Karki, M. C. Warren, L. Stixrude, G. J. Ackland, and J. Crain, *Phys. Rev. B* **55**, 3465-3471 (1997).
 - ³⁷ M. Murakami, K. Hirose, K. Kawamura, N. Sata, and Y. Ohishi, *Science* **304**, 855-858 (2004).
 - ³⁸ A. R. Oganov and S. Ono, *Nature* **430**, 445448 (2004).
 - ³⁹ T. Tsuchiya, J. Tsuchiya, K. Umemoto, and R. M. Wentzcovitch, *Earth Planet. Sci. Lett.* **224**, 241-248 (2004).
 - ⁴⁰ Marc Javoy, Francoise Pineau, and Claude J. Allegre, *Nature* **300**, 171-173 (1982).
 - ⁴¹ B. Marty and A. Jambon, *Earth Planet. Sci. Lett.* **83**, 16-26 (1987).
 - ⁴² N. L. Dobretsov and A. F. Shatskiy, *Russian Geology and Geophysics* **53**, 1117-1132 (2012).
 - ⁴³ D. P. Schrag, John. A. Higgins, Francis A. Macdonald, and David T. Johnston, *Science* **339**, 540 (2013).
 - ⁴⁴ P. Deines, *Earth-Science Reviews* **58**, 247-278 (2002).